Electronic Supplementary Information (ESI)

Inorganic/organic hybrid solar cells: Optimal carrier transport in vertically-aligned silicon nanowire arrays

Keisuke Sato,[*ab] Mrinal Dutta[a] and Naoki Fukata[*a]

[a]World Premier International Research Center for Materials Nanoarchitectonics, National Institute for Materials Science, 1-1 Namiki, Tsukuba, Ibaraki 305-0044, Japan
[b]Department of Electrical and Electronic Engineering, Tokyo Denki University, 5 Senju-Asahi-cho, Adachi-ku, Tokyo 120-8551, Japan
E-mail: satok@mail.dendai.ac.jp, FUKATA.Naoki@nims.go.jp

Experimental

Fabrication of planar Si/PEDOT:PSS hybrid heterojunction solar cell

The n-type Si (111) wafers with a resistivity of 1 - 50 Ωcm and sized 15 × 15 mm were used as the starting substrates. The Si wafers were sequentially cleaned with acetone, ethanol and deionized water for 10 min each. As the final part of cleaning, they were cleaned with piranha solution for 50 min, followed by dilute HF acid for 2 min to remove any native oxide and allow the wafer surface to become hydrophobic. Immediately after this cleaning step, highly conductive PEDOT:PSS mixed with 5 wt% DMSO and 0.1 wt% Zonyl fluorosurfactant was spin-coated onto the wafer surface at 7500 rpm for 120 s in air to form the planar hybrid solar cell consisting of Si/PEDOT:PSS heterojunction, followed by annealing at 140 ºC for 30 min in ambient atmosphere to remove any residual water inside the PEDOT:PSS. To complete the hybrid solar cells with an active area of 25 mm^2, a 100-nm-thick silver finger-grid electrode was deposited on the surface of the PEDOT:PSS by DC sputtering through a shadow mask, while a 100-nm-thick aluminum electrode was deposited by DC sputtering onto the back side of the wafer after the HF acid cleaning. The width of each finger of silver grid electrode was 100 μm, and the spacing between fingers was 500 μm. As the final stage of the process, the fabricated solar cells were annealed at 150 - 250 ºC in a nitrogen atmosphere for 30 min.

Characterization

Fourier transform infrared (FTIR) measurement was carried out at room temperature using a Thermo Electron Nicolet 4700 FTIR spectrometer to characterize the surface conditions of NW arrays with different lengths before and after HF acid process. Electron spin resonance (ESR) measurement was performed using a JEOL JES-FA200 X-band spectrometer at room temperature to investigate the defects in the NW arrays with different lengths before and after HF acid process. The *g* value was determined using the signals of Mn^{2+}. To demonstrate the contact type of silver electrode on the PEDOT:PSS layer and aluminum electrode on the back side of the Si wafer before and after annealing at 200 ºC for 30 min, current-voltage characteristics between silver electrodes deposited on the surface of the PEDOT:PSS layer and between aluminum electrodes deposited on the back side of the Si wafer were measured at room temperature. The size of each silver electrode and each aluminum electrode is 4 × 4 mm, and their thickness is 100 nm. The distance between their electrodes is 5 mm from center to center. To characterize the thermal stability of the PEDOT:PSS layer, thermogravimetry-differential thermal analysis (TG-DTA) was carried out using a SII Exstar TG/DTA6200.

Morphology of vertically-aligned SiNW arrays formed at different etching time

The morphology of SiNW arrays fabricated by metal-assisted chemical etching for various etching time was confirmed by SEM. Fig. S1 presents the 5º tilted cross-sectional view SEM micrograph of SiNW arrays fabricated for different etching time. The vertically-aligned SiNW arrays can be clearly seen in all the samples. The NW length was controlled from 0.2 to 0.57, 2.1 μm with the increase in the etching time from 1 to 3, 12 min, respectively (Fig. S1a-c). As a nature of the metal-assisted chemical etching method, the NW arrays with the longer lengths of 2.1 μm tend to aggregate at their top portion and form the bundles. Therefore, the 2.1 μm-NW arrays are composed of bunched NW configurations (Fig. S1c) rather than individual NW configurations, which were observed from the NW arrays with lengths shorter than 0.57 μm (Fig. S1a and b).

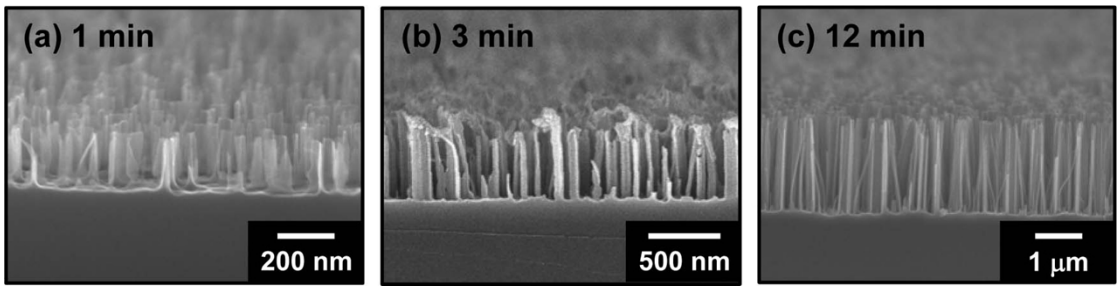

Fig. S1 5º tilted cross-sectional view SEM images of vertically-aligned SiNW arrays obtained by metal-assisted chemical etching for (a) 1 min, (b) 3 min and (c) 12 min.

Correlation between surface conditions and defects in the SiNW arrays with different lengths before and after HF acid process

FTIR and ESR analyses were performed to characterize the surface conditions and defects in the SiNW arrays with different lengths before and after HF acid process. Fig. S2a and c show the FTIR spectra of NW arrays with different lengths before and after HF acid process, respectively, while Fig. S2b and d show the ESR spectra of their corresponding NW arrays. All the NW arrays before HF acid process exhibited only the peaks around 804, and 1110 and 1220 cm^{-1} derived from symmetric and asymmetric Si-O stretching modes,[1-3] respectively, meaning the NW surface is surrounded by the oxide layer (Fig. S2a). Due to the presence of surface oxide layer, the interfacial defects between the crystalline Si core constituting the NW and surface oxide layer, which are so-called P_b centers with a g value of 2.006,[4] were formed for all the NW arrays before HF acid process (Fig. S2b). When the NW surfaces were cleaned with dilute HF acid, the peaks around 663, 910 and 2100 cm^{-1} derived from Si-H deformation mode,[5] Si-H_2 scissors mode[5] and Si-H stretching mode,[5] respectively, were detected, in addition to the peak due to slight asymmetric Si-O stretching mode around 1110 cm^{-1} (Fig. S2c). This result indicates that the hydrogen termination onto the NW surface by the HF acid process leads to the removal of interfacial defects (Fig. S2d). Therefore, the FTIR and ESR results clearly demonstrate that any defects on the NW surface after HF acid process are passivated with hydrogen.

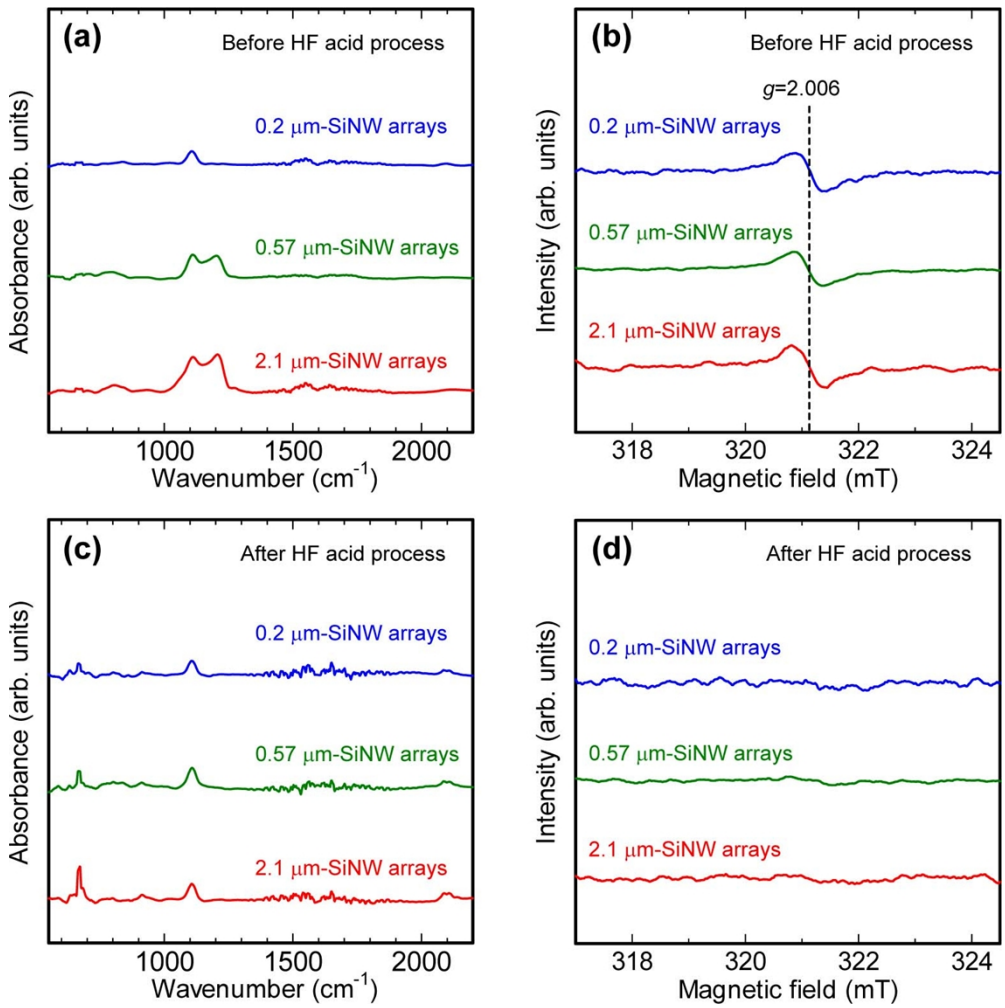

Fig. S2 (a and c) FTIR and (b and d) ESR spectra of SiNW arrays with different lengths before (upper) and after (bottom) HF acid process.

Current-voltage characteristics of silver electrode on the PEDOT:PSS layer and aluminum electrode on the back side of Si wafer

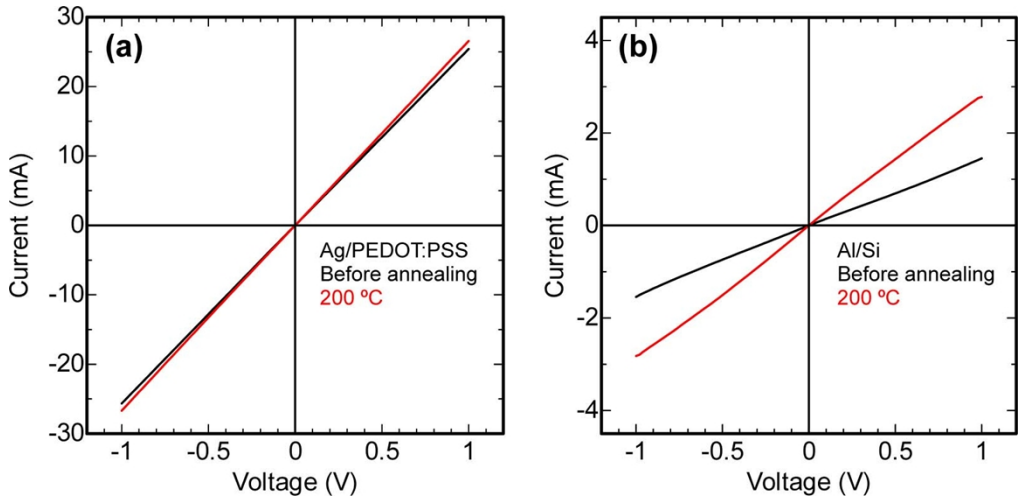

Fig. S3 Current-voltage characteristics (a) between silver electrodes on the surface of the PEDOT:PSS layer and (b) between aluminum electrodes on the back side of the Si wafer before and after annealing at 200 ºC.

Magnified HRTEM image of 0.57 μm-individual SiNW/PEDOT:PSS hybrid structure

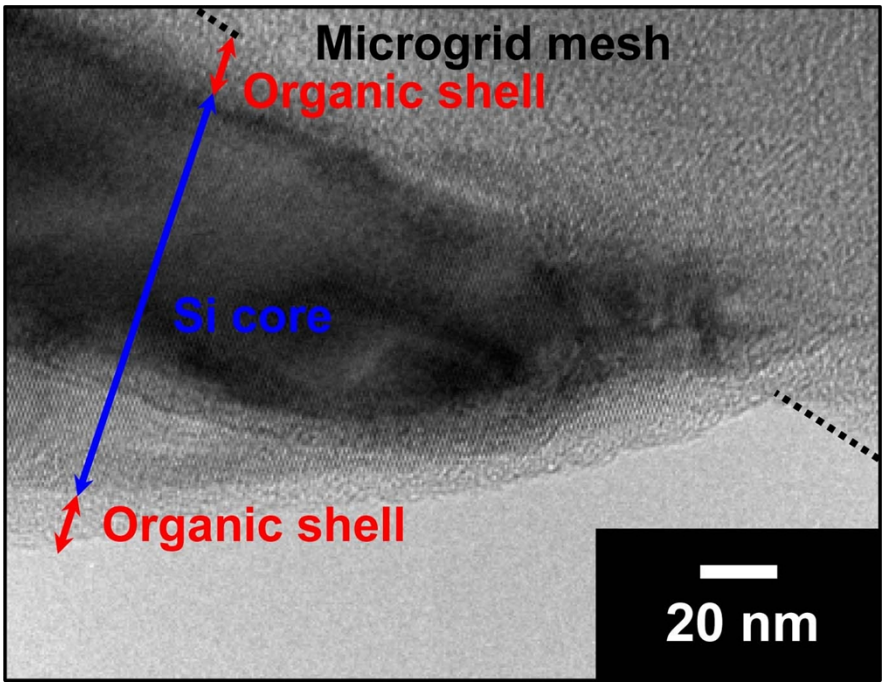

Fig. S4 Magnified image of HRTEM micrograph shown in Fig. 1(d).

Morphology of SiNW/PEDOT:PSS hybrid structures with different lengths after annealing at 200 ºC

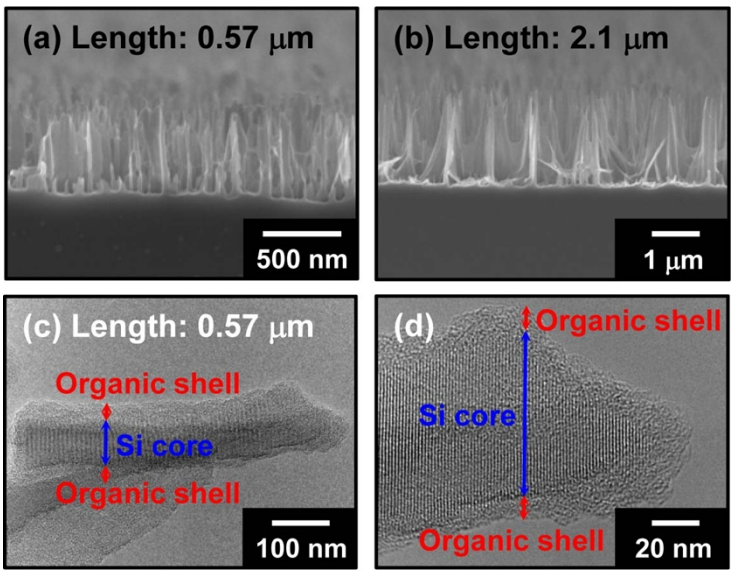

Fig. S5 5º tilted cross-sectional view SEM images of SiNW/PEDOT:PSS hybrid structures with length of (a) 0.57μm and (b) 2.1 μm after annealing at 200 ºC. (c) Plain-view HRTEM image of 0.57μm-individual SiNW/PEDOT:PSS hybrid structure after annealing at 200 ºC. (d) Highly magnified HRTEM image of (c).

Reflectance and optical absorption properties of SiNW/PEDOT:PSS hybrid structures with different lengths after annealing at 200 ºC

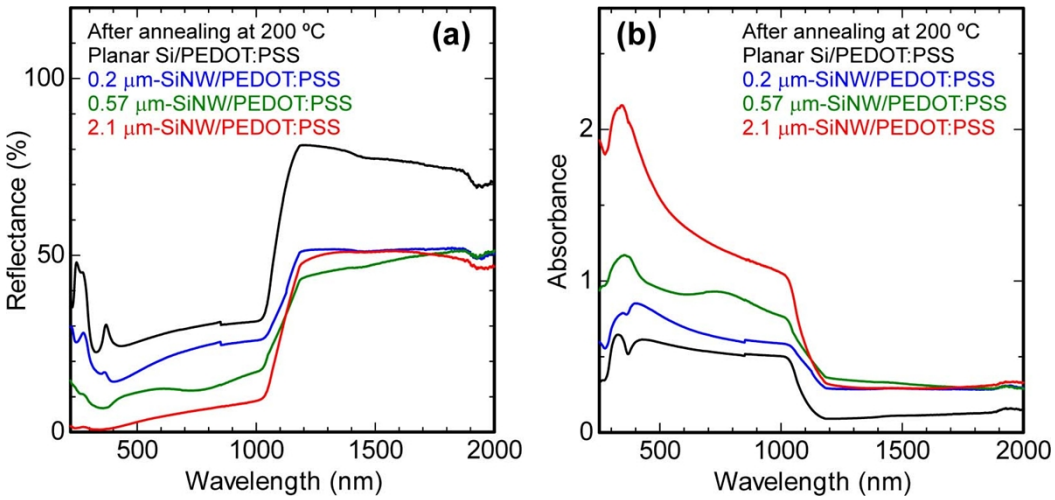

Fig. S6 (a) Reflectance and (b) optical absorption spectra of planar Si/PEDOT:PSS hybrid structure and SiNW/PEDOT:PSS hybrid structures with different lengths after annealing at 200 ºC.

Electrical conductivity and transmittance of silver electrodes with different film thicknesses after annealing

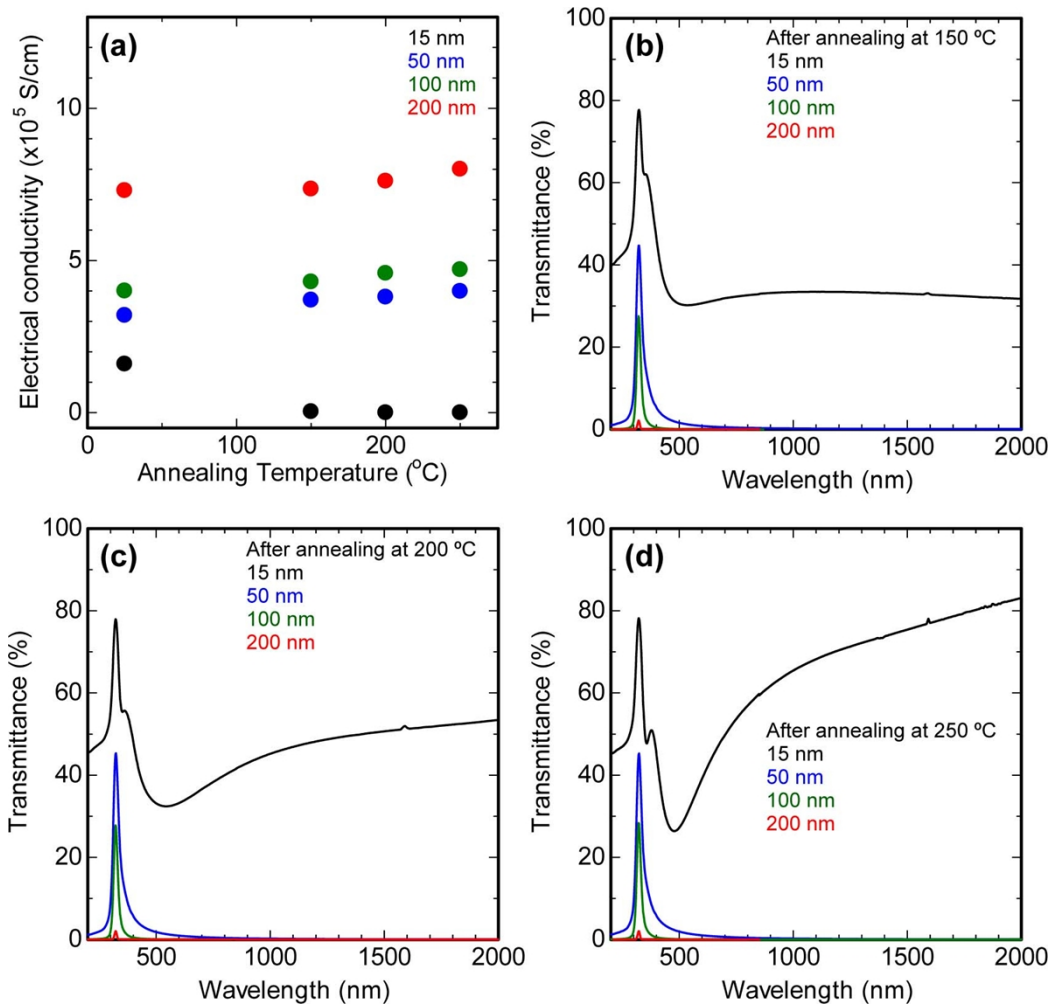

Fig. S7 (a) Electrical conductivities of silver electrodes with different film thicknesses as a function of annealing temperature. Transmittance of silver electrodes with different film thicknesses after annealing at (b) 150 ºC, (c) 200 ºC and (d) 250 ºC.

Electrical conductivity of 100-nm-thick aluminum electrode after annealing

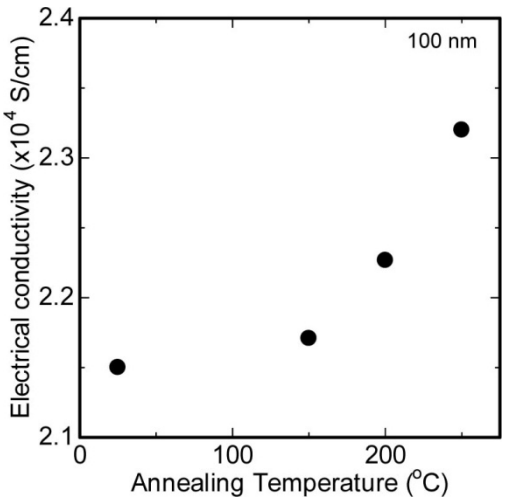

Fig. S8 Electrical conductivity of 100-nm-thick aluminum electrode as a function of annealing temperature.

TG-DTA measurements of PEDOT:PSS layer

TG-DTA measurements were performed to characterize the thermal stability of the PEDOT:PSS layer. Fig. S9 presents the TG-DTA spectrum of the PEDOT:PSS layer. The PEDOT:PSS layer mainly exhibited two weight loss stages. In the temperature range from room temperature to 150 ºC, 13 wt% weight losses were detected and an endothermic peak also appeared at 80 ºC. The detection of weight loss is related to the removal of residual water and solvents inside the PEDOT:PSS due to the endothermic reaction. Therefore, the primary weight loss is caused by the endothermic decomposition of the PEDOT:PSS layer. As the temperature is increased from 150 to 200 ºC, the PEDOT:PSS layer exhibited the negligible weight loss less than 2.1 wt%. This indicates that the thermal decomposition of the PEDOT:PSS layer is inhibited in this temperature range. At the final stage in the temperature range from 200 to 300 ºC, the secondary weight loss occurred. The weight loss of the PEDOT:PSS layer at 300 ºC was increased to 22 wt% from 15.1 wt%, which is that at 200 ºC. Moreover, an exothermic peak was also observed around 230 ºC. The exothermic reaction induces the carbonization of polymer due to the decomposition of the PEDOT:PSS layer, resulting in the performance deterioration of the PEDOT:PSS. Therefore, the secondary weight loss is caused by the exothermic decomposition of the PEDOT:PSS layer.

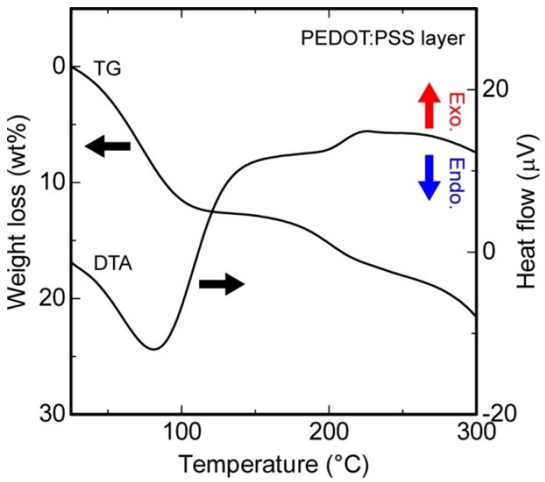

Fig. S9 TG-DTA curve of the PEDOT:PSS layer.

Electrical conductivity and transmittance of silver electrodes with different film thicknesses

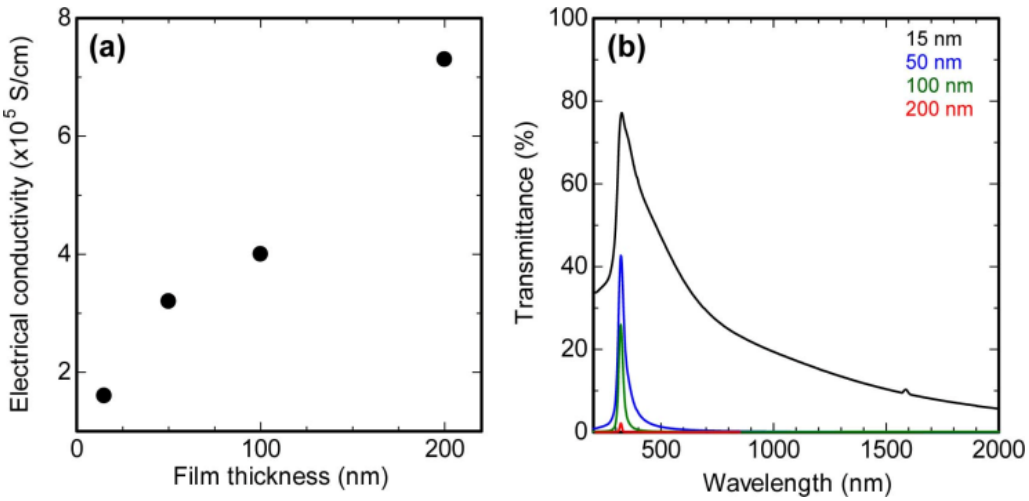

Fig. S10 (a) Electrical conductivities and (b) transmittance of silver electrodes with different film thicknesses.

References

1. R. D. Tilley, J. H. Warner, K. Yamamoto, I. Matsui and H. Fujimori, *Chem. Commun*., 2005, 1833-1835.
2. C. Fang, N. Bhattarai, C. Sun and M. Zhang, *Small*, 2009, 5, 1637-1641.
3. K. Sato, K. Niino, N. Fukata, K. Hirakuri and Y. Yamauchi, *Nanotechnology*, 2009, 20, 365207.
4. N. Fukata, S. Ishida, S. Yokono, R. Takiguchi, J. Chen, T. Sekiguchi and K. Murakami, *Nano Lett*., 2011, 11, 651-656.
5. E. C. Wu, J.-H. Park, J. Park, E. Segal, F. Cunin and M. J. Sailor, *ACS Nano*, 2008, 2, 2401-2409.